Research Article | Vol. 25, No. 26 | 25 Dec 2017 | OPTICS EXPRESS 32323
Optics EXPRESS

Bragg gratings in thin-film $LiNbO_3$ waveguides

MOHAMMAD AMIN BAGHBAN,[1] JEAN SCHOLLHAMMER,[1] CARLOS ERRANDO-HERRANZ,[2] KRISTINN B. GYLFASON,[2] AND KATIA GALLO[1,*]

[1]*Department of Applied Physics, KTH Royal Institute of Technology, Roslagstullsbacken 21, Stockholm SE-106 91, Sweden*
[2]*Department of Micro and Nanosystems, KTH Royal Institute of Technology, Osquldas väg 10, Stockholm SE-100 44, Sweden*
**gallo@kth.se*

Abstract: We design, fabricate and characterize sidewall corrugated Bragg gratings in a high confinement integrated optics lithium niobate platform, comprising submicrometric photonic wires, tapers and grating couplers to interface off-chip standard telecom optical fibers. We analyze the grating performance as band-rejection filter for TE-polarized signals in the telecom C-band, considering both rectangular and sinusoidal sidewall profiles, and demonstrate record extinction ratios as high as 27 dB and rejection bandwidths as narrow as 3 nm. The results show the potential for an efficient integration of novel photonic functionalities into low-footprint $LiNbO_3$ nonlinear and electro-optical waveguide devices.

OCIS codes: (130.3730) Lithium niobate; (130.3120) Integrated optics devices; (230.1480) Bragg reflectors; (310.6845) Thin film devices and applications; (230.7370) Waveguides.

References and links

1. C. Caucheteur, T. Guo, and J. Albert, "Polarization-Assisted Fiber Bragg Grating Sensors: Tutorial and Review," J. Lightwave Technol. **35**(16), 3311–3322 (2017).
2. G. D. Marshall, R. J. Williams, N. Jovanovic, M. J. Steel, and M. J. Withford, "Point-by-point written fiber-Bragg gratings and their application in complex grating designs," Opt. Express **18**(19), 19844–19859 (2010).
3. D. T. Spencer, M. Davenport, S. Srinivasan, J. Khurgin, P. A. Morton, and J. E. Bowers, "Low kappa, narrow bandwidth Si_3N_4 Bragg gratings," Opt. Express **23**(23), 30329–30336 (2015).
4. C. Klitis, G. Cantarella, M. J. Strain, and M. Sorel, "High-extinction-ratio TE/TM selective Bragg grating filters on silicon-on-insulator," Opt. Lett. **42**(15), 3040–3043 (2017).
5. P. Millar, R. M. De La Rue, T. F. Krauss, J. S. Aitchison, N. G. R. Broderick, and D. J. Richardson, "Nonlinear propagation effects in an AlGaAs Bragg grating filter," Opt. Lett. **24**(10), 685–687 (1999).
6. L. E. Myers, R. C. Eckardt, M. M. Fejer, R. L. Byer, W. R. Bosenberg, and J. W. Pierce, "Quasi-phase-matched optical parametric oscillators in bulk periodically poled $LiNbO_3$," J. Opt. Soc. Am. B **12**(11), 2102–2116 (1995).
7. M. A. Baghban and K. Gallo, "Impact of longitudinal fields on second harmonic generation in lithium niobate nanopillars," APL Photonics **1**(6), 061302 (2016).
8. C. Langrock, S. Kumar, J. E. McGeehan, A. E. Willner, and M. M. Fejer, "All-Optical Signal Processing Using $\chi^{(2)}$ Nonlinearities in Guided-Wave Devices," J. Lightwave Technol. **24**(7), 2579–2592 (2006).
9. J. Wang, F. Bo, S. Wan, W. Li, F. Gao, J. Li, G. Zhang, and J. Xu, "High-Q lithium niobate microdisk resonators on a chip for efficient electro-optic modulation," Opt. Express **23**(18), 23072–23078 (2015).
10. K. De Greve, L. Yu, P. L. McMahon, J. S. Pelc, C. M. Natarajan, N. Y. Kim, E. Abe, S. Maier, C. Schneider, M. Kamp, S. Höfling, R. H. Hadfield, A. Forchel, M. M. Fejer, and Y. Yamamoto, "Quantum-dot spin-photon entanglement via frequency downconversion to telecom wavelength," Nature **491**(7424), 421–425 (2012).
11. M. Picciau, G. Leo, and G. Assanto, "Versatile bistable gate based on quadratic cascading in a Bragg periodic structure," J. Opt. Soc. Am. B **13**(4), 661–670 (1996).
12. C. Conti, S. Trillo, and G. Assanto, "Doubly Resonant Bragg Simultons via Second-Harmonic Generation," Phys. Rev. Lett. **78**(12), 2341–2344 (1997).
13. J. Hukriede, D. Runde, and D. Kip, "Fabrication and application of holographic Bragg gratings in lithium niobate channel waveguides," J. Phys. D Appl. Phys. **36**(3), R1–R16 (2003).
14. S. Kroesen, W. Horn, J. Imbrock, and C. Denz, "Electro-optical tunable waveguide embedded multiscan Bragg gratings in lithium niobate by direct femtosecond laser writing," Opt. Express **22**(19), 23339–23348 (2014).
15. B. K. Das, R. Ricken, V. Quiring, H. Suche, and W. Sohler, "Distributed feedback-distributed Bragg reflector coupled cavity laser with a Ti:(Fe:)Er:$LiNbO_3$ waveguide," Opt. Lett. **29**(2), 165–167 (2004).
16. C. Guyot, G. Ulliac, J. Dahdah, W. Qiu, M.-P. Bernal, F. Baida, and N. Courjal, "Optical characterization of ultra-short Bragg grating on lithium niobate ridge waveguide," Opt. Lett. **39**(2), 371–374 (2014).

#308265 https://doi.org/10.1364/OE.25.032323
Journal © 2017 Received 3 Oct 2017; revised 9 Dec 2017; accepted 9 Dec 2017; published 12 Dec 2017

Optics EXPRESS

17. B. E. Benkelfat, R. Ferriere, B. Wacogne, and P. Mollier, "Technological implementation of Bragg grating reflectors in Ti:$LiNbO_3$ waveguides by proton exchange," IEEE Photonics Technol. Lett. **14**(10), 1430–1432 (2002).
18. P. Rabiei and P. Gunter, "Optical and electro-optical properties of submicrometer lithium niobate slab waveguides prepared by crystal ion slicing and wafer bonding," Appl. Phys. Lett. **85**(20), 4603–4605 (2004).
19. G. Poberaj, H. Hu, W. Sohler, and P. Günter, "Lithium niobate on insulator (LNOI) for micro-photonic devices," Laser Photonics Rev. **6**(4), 488–503 (2012).
20. H. Hu, R. Ricken, and W. Sohler, "Lithium niobate photonic wires," Opt. Express **17**(26), 24261–24268 (2009).
21. S. Y. Siew, S. S. Saha, M. Tsang, and A. J. Danner, "Rib Microring Resonators in Lithium Niobate on Insulator," IEEE Photonics Technol. Lett. **28**(5), 573–576 (2016).
22. R. Luo, H. Jiang, S. Rogers, H. Liang, Y. He, and Q. Lin, "On-chip second-harmonic generation and broadband parametric down-conversion in a lithium niobate microresonator," Opt. Express **25**(20), 24531–24539 (2017).
23. H. Lu, B. Sadani, N. Courjal, G. Ulliac, N. Smith, V. Stenger, M. Collet, F. I. Baida, and M. P. Bernal, "Enhanced electro-optical lithium niobate photonic crystal wire waveguide on a smart-cut thin film," Opt. Express **20**(3), 2974–2981 (2012).
24. S. Diziain, R. Geiss, M. Zilk, F. Schrempel, E.-B. Kley, A. Tünnermann, and T. Pertsch, "Second harmonic generation in free-standing lithium niobate photonic crystal L3 cavity," Appl. Phys. Lett. **103**(5), 051117 (2013).
25. L. Cai, S. Zhang, and H. Hu, "A compact photonic crystal micro-cavity on a single-mode lithium niobate photonic wire," J. Opt. **18**(3), 035801 (2016).
26. M. Mahmoud, S. Ghosh, and G. Piazza, "Lithium Niobate on Insulator (LNOI) Grating Couplers," in *CLEO: 2015*, OSA Technical Digest (online) (Optical Society of America, 2015), SW4I.7.
27. M. S. Nisar, X. Zhao, A. Pan, S. Yuan, and J. Xia, "Grating Coupler for an On-Chip Lithium Niobate Ridge Waveguide," IEEE Photonics J. **9**(1), 1–8 (2017).
28. C. Wang, X. Xiong, N. Andrade, V. Venkataraman, X.-F. Ren, G.-C. Guo, and M. Lončar, "Second harmonic generation in nano-structured thin-film lithium niobate waveguides," Opt. Express **25**(6), 6963–6973 (2017).
29. F. Morichetti, A. Canciamilla, C. Ferrari, M. Torregiani, A. Melloni, and M. Martinelli, "Roughness Induced Backscattering in Optical Silicon Waveguides," Phys. Rev. Lett. **104**(3), 033902 (2010).
30. H. Nishihara, M. Haruna, and T. Suhara, *Optical Integrated Circuits* (McGraw-Hill, 1989).
31. A. Yariv and M. Nakamura, "Periodic structures for integrated optics," IEEE J. Quantum Electron. **13**(4), 233–253 (1977).
32. J. Hong, W. Huang, and T. Makino, "On the transfer matrix method for distributed-feedback waveguide devices," J. Lightwave Technol. **10**(12), 1860–1868 (1992).

1. Introduction

The Bragg grating is a fundamental component for functional optical devices developed in a variety of photonic platforms (optical fibers [1, 2], silicon [3, 4], and other semiconductors [5]) with applications as diverse as communications, lasers, and sensing. The functionalities afforded by Bragg grating filters and reflectors are particularly appealing when combined with the nonlinear optical and electro-optic features of materials such as lithium niobate ($LiNbO_3$, LN), routinely exploited for frequency conversion [6, 7], optical switching, modulation [8, 9] and quantum optics [10]. All such applications could greatly benefit from the possibility of embedding the functionalities of Bragg grating reflectors and filters in LN waveguides, as this might enable ultra-compact electrically-tunable optical switches and modulators as well as low-footprint nonlinear photonic devices such as optical parametric oscillators. Furthermore, a technology affording high-quality Bragg gratings in LN waveguides would be pivotal for novel device concepts relying on the interplay between quadratic nonlinearities and the feedback provided by a periodic perturbation, still awaiting experimental demonstration [11, 12].

Progress in this direction has so far been hampered by the difficulty of achieving reliable patterning at sub-micrometric scales of high-contrast periodic refractive index structures in LN. Even the best Bragg gratings fabricated to date in LN, implemented with laser exposure, proton-exchange or focused-ion-beam-milling technologies [13–17], still suffer from either limited index contrasts or reduced lengths restricting their performance with respect to what are nowadays routine achievements for Bragg gratings in silicon on insulator (SOI) waveguides, featuring extinction ratios in excess of 20 dB, bandwidths of a few nanometers and operation in strong coupling (high-kappa) regimes [4].

The advent of thin-film lithium niobate on insulator (LNOI) platforms [18,19] has changed this scenario, by providing a platform suitable for the implementation of high-

Optics EXPRESS

confinement photonic nanowires [20], microdisc and microring resonators [9, 21, 22], photonic crystals [23–25] and integrated grating couplers [26, 27], similar to those routinely achieved in silicon photonics. Moreover, the tight confinement attainable with LNOI high-contrast waveguides makes it possible to envisage strong submicrometric-pitch gratings operating in strong coupling regimes, for both surface and sidewall corrugated structures, comparable with SOI counterparts [16].

Here, we demonstrate record extinction ratios (27 dB) in integrated Bragg gratings implemented in LNOI submicrometric photonic waveguides, operating at telecom wavelengths in the strong grating coupling regime with lengths of 0.25 and 0.5 mm. The structures are all implemented in one Electron-Beam Lithography (EBL) step, whereby submicrometric waveguides and Bragg sidewall gratings, as well as surface corrugated grating couplers and tapers enabling in/out fiber coupling, are fabricated simultaneously. The overall footprint of each on-chip device is 12×1800 μm^2.

In this study we also explore a range of different grating profiles and parameters, providing guidelines for further optimization. The results hold promise for novel compact photonic devices exploiting the functionalities of Bragg gratings in combination with the electro-optical and nonlinear-optical features of high-confinement LN waveguides for ultrafast signal processing, quantum computing and sensing applications.

2. Device structure

2.1 Fabrication

Integrated optical structures were fabricated according to the process steps outlined in Fig. 1. The starting point was a commercial thin-film LNOI wafer (Partow Technologies LLC), consisting of a 300 nm-thick *Y*-cut LN slab bonded to silicon by a 2 μm-thick SiO_2 layer [Fig. 1(a)]. The intrinsic propagation loss of the slab at a wavelength of 1550 nm was 3 dB/cm.

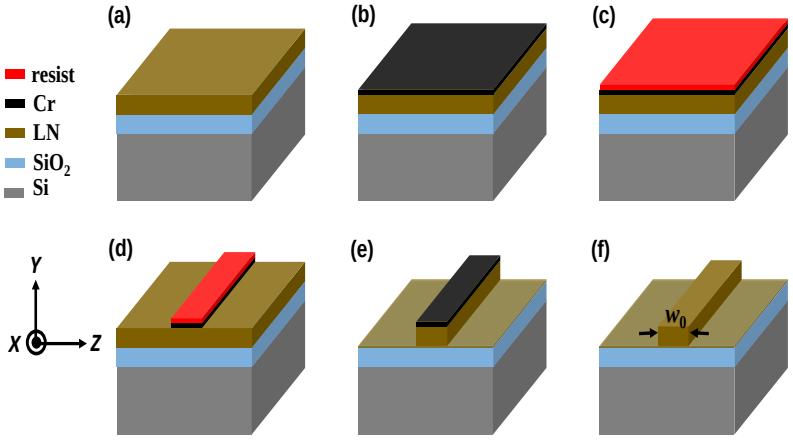

Fig. 1. Schematic representation of the fabrication process: (a) LNOI chip, as purchased; (b) Chromium (Cr) hard mask deposition; (c) Electron-beam resist spin-coating; (d) EBL and etching Cr hard mask by Cl_2/O_2 reactive ion etching; (e) Ar + ion milling of LN; (f) Cr mask removal by wet etch. The arrows illustrate the LN crystallographic axes (*X*, *Y*, *Z*).

All integrated optics components, i.e. grating couplers, tapers, photonic waveguides and Bragg gratings (see also section 2.2) were realized in a single EBL step on 0.8×1.3 cm^2 LNOI chips. A 200 nm-thick chromium film, deposited on the thin film LN layer by electron-beam evaporation (Fig. 1(b)), served as hard mask for the etching of LN. EBL was performed by a Raith 150 TK system, using a negative resist [Fig. 1(c)]. The resist pattern was then transferred into a chromium hard mask via reactive ion etching (Oxford Plasmalab 100) in a mixture of Cl_2 and O_2 gases at room temperature (Figs. 1(d) and 1(e)). 270 nm-deep devices were then etched into the LN layer by Ar^+ ion milling at a temperature of –50°C and a

Optics EXPRESS

pressure of 7 mTorr [Fig. 1(e)]. Finally, the residual chromium mask layer was removed by wet etching in a ceric ammonium nitrate solution [Fig. 1(f), illustrating the cross-section of a nanowire of width w_0]. The etched LN structures had an angle of 45°.

2.2 Device layout

The top view of the basic layout of an integrated LNOI Bragg grating device is schematically shown in Fig. 2(a). It consists of a strip waveguide of width w_0 and length L_W, with an embedded Bragg grating of length L_B, and additional input and output couplers made of uniform gratings and tapered waveguide sections, to interface the LNOI photonic waveguides with off-chip standard telecom single mode fibers.

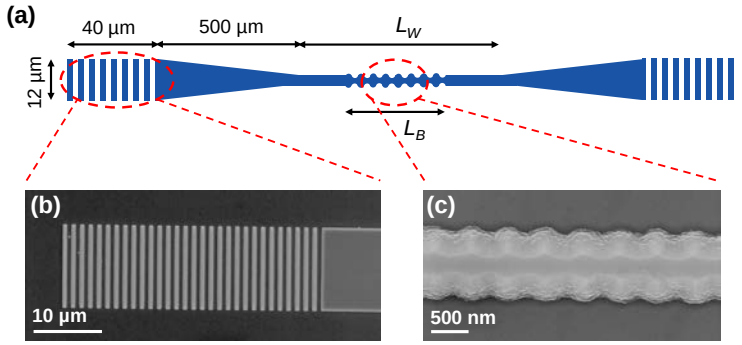

Fig. 2. (a) Schematic illustration of the fabricated devices, where L_W is the total length of the nano-waveguide and L_B the length of the Bragg grating. (b) Scanning electron microscope (SEM) image of a fabricated (relief) grating coupler with a period of Λ_C = 1.24 µm and a duty cycle of 50%; (c) SEM image of a fabricated (sidewall) Bragg grating of period Λ_B = 505 nm, sidewall corrugation Δw = 125 nm and average waveguide width w_0 = 760 nm.

Multiple devices of the kind of Fig. 2(a) were fabricated in a single lithographic step as described in Fig. 1. All devices employed the same coupler design for TE-polarized optical signals, consisting of etched-through surface gratings of constant period (Λ_C = 1.24 µm) inscribed into 12 µm-wide and 40 µm-long waveguide sections (Fig. 2(b)). The latter were tapered down over a fixed length (500 µm), to match the width of each targeted photonic wire.

All photonic waveguides were aligned to the *X* crystallographic axis of LN. Due to the uniaxial nature of LN, the same results are expected for waveguides aligned to the *Y* crystallographic axis in *X*-cut LNOI-on-$LiNbO_3$. Each chip included multiple sets of devices of the kind of Fig. 2(a), with different nominal waveguide widths w_0 (ranging from 760 nm to ~2.5 µm) and lengths L_W (ranging from 0.5 to 4 mm). As for the Bragg gratings, we employed sidewall-modulated structures with sinusoidal and rectangular corrugations of different length (L_B ~250 and ~500 µm) and amplitude (Δw ranging from 50 to 125 nm), with a fixed period (Λ_B = 505 nm). Figure 2(c) shows the detail of a sinusoidal Bragg grating with Δw = 125 nm, embedded in a 760 nm-wide waveguide.

3. Experimental results

All devices in this study operated with TE-polarized fundamental modes at telecom wavelengths and were characterized by using a fiber-coupled experimental setup, as shown in Fig. 3(a). A tunable continuous-wave laser, together with a fiber polarization controller, was used to provide a TE-polarized input signal for the grating couplers on-chip, operating at a fixed incidence angle (θ = 10°, Fig. 3(b)). The output from each waveguide was collected off-chip through a standard telecom fiber by a similar grating coupler structure after manual adjustments for maximum throughput. The spectral response of each device was recorded by an optical spectrum analyzer (OSA), synchronized with the tunable continuous-wave laser.

Optics EXPRESS

The OSA was typically operated with a spectral resolution of ~10 pm and a reference level of −25 dB.

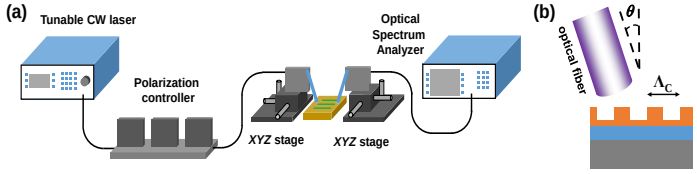

Fig. 3. (a) Schematic illustration of the setup used for experiments; and (b) schematic side-view of employment of grating couplers with a period of Λ_C = 1.24 μm for in- and out-coupling of optical signals.

In order to extrapolate the intrinsic response of the Bragg gratings from measurements made on the full devices [comprising also input and output couplers and tapers, Fig. 2(a)], the response of the couplers and of the straight LNOI photonic waveguide sections were first assessed in a separate set of experiments, discussed in the next section.

3.1 Grating couplers and photonic wire waveguides

To determine the propagation losses of the waveguides and the grating coupling efficiencies, systematic measurements were first performed on separate sets of waveguides of different lengths L_W (Fig. 2(a)), without the Bragg gratings, fabricated on the same chip. Figure 4(a) compares experimental results obtained at fixed wavelength (λ = 1550 nm) for two different waveguide widths (w_0 = 760 nm and w_0 = 2.35 μm).

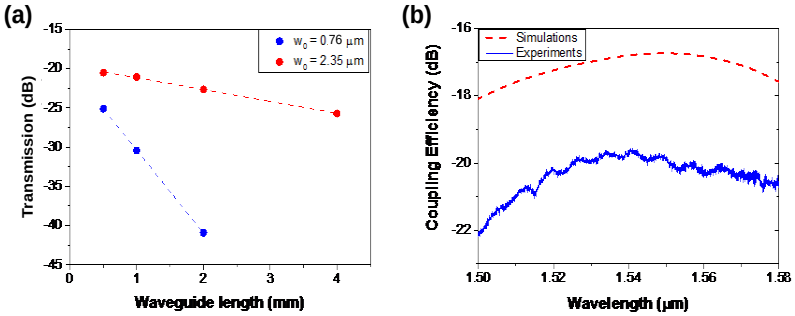

Fig. 4. (a) Optical fiber-to-fiber transmission measured at λ = 1550 nm for TE-polarized light, in 760 nm- (blue circles) and 2.35 μm-wide (red circles) LNOI waveguides. Dashed lines represent linear fittings performed on experimental data. (b) Spectral response of the fabricated grating couplers in the telecom range, obtained by simulations and experiments (dashed and solid lines, respectively).

The figure shows the fiber-to-fiber transmission of the full device (i.e. nanowire waveguide + input and output couplers and tapers), plotted in logarithmic scale as a function of waveguide length, L_W. The experimental points (red and blue markers) exhibit a linear trend when plotted in log scale, which is consistent with an expected functional dependence of the transmission on the waveguide length (L_W) of the form: $\sim e^{-\alpha L_W}$. This allows to estimate the propagation loss coefficient (α) through a linear fit of the experimental data (dashed lines in Fig. 4(a)), yielding α = 76.2 ± 5.14 dB/cm and 15.1 ± 0.51 dB/cm for 760 nm- and 2.35 μm-wide waveguides, respectively. Such relatively high values might be significantly reduced by resorting to LNOI-on-$LiNbO_3$ wafers exhibiting lower intrinsic losses [20], and by further optimization of the nanowire fabrication process [28]).

Furthermore, the linear extrapolation of the transmission data for $L_W \to 0$ allows to readily estimate the total coupling efficiency of the grating couplers, yielding an experimental value equal to −19.9 dB, independent of the waveguide width. This allows to attribute to each

Optics EXPRESS

integrated coupler (grating + taper) a constant loss term, amounting to 9.95 dB and further suggests that the tapers are selectively exciting only the fundamental TE_{00} mode of the photonic waveguides, even in those cases when the latter can support several guided modes (i.e. for $w_0 > 1.1$ μm).

Figure 4(b) illustrates the spectral response of the couplers, measured here with a 760 nm-wide waveguide of length L_W = 2 mm. After the correction for waveguide propagation losses (determined with the procedures outlined before), the experimental data (blue line) appear in fairly good agreement with the simulations (red dashed lines). The grating couplers exhibit a broadband response, with a 3dB bandwidth in excess of 80 nm (limited by experimental capabilities). The wavelength at which the grating coupler exhibits its highest efficiency is slightly shifted with respect to the theoretical prediction (λ = 1550 nm), which might be due to slight fabrication imperfections affecting the duty cycle of the grating. The experimental results exhibit a maximum coupling efficiency of –19.9 dB for the input/output coupler pair (including gratings and tapers). This value is to be compared with the theoretical one of –16.74 dB, obtained from numerical simulations (commercial FDTD solver, Lumerical) done for the gratings without tapers. The residual ~3 dB difference between the theory and experiment can be reasonably ascribed to the additional propagation losses introduced by the narrower sections of the tapers which were not accounted for by the simulations, and to possible imperfections in the fabrication of the grating couplers with respect to the design.

3.2 Bragg gratings

The performance of the Bragg gratings as band-rejection filters at telecom wavelengths were analyzed next. We considered devices where the waveguide width was modulated with a constant period (Λ_B) along the propagation axis (x) over a fixed length (L_B), i.e. $w(x) = w_0 + \Delta w\, f(x)$, Δw being the corrugation amplitude and $f(x)$ the periodic function which defines the grating sidewall modulation. Accordingly, for the case of rectangular and sinusoidal Bragg gratings [Figs. 5(a) and 5(b)]: $f(x) = \left[rect\left(\frac{2x}{\Lambda_B} - 2m\right) - rect\left(\frac{2x}{\Lambda_B} - 2m - 1\right)\right]$ with m being a non-negative integer and $f(x) = sin\left(\frac{2\pi x}{\Lambda_B}\right)$, respectively. Figures 5(c) and 5(d) show the normalized transmission spectra retrieved from the experiments for the two grating types, corrected for waveguide coupling and propagation losses (as discussed in sect. 3.1) by removing the grating coupler response and propagation loss from the measurements. In both cases the gratings have a period of Λ_B = 505 nm and a length of L_B = 252.5 μm (i.e. 500 Bragg periods). Each figure compares the response retrieved from the experiments for four different values of corrugation amplitude, i.e.: Δw = 50, 75, 100 and 125 nm. The average waveguide widths are w_0 = 700 nm and 760 nm for the rectangular [Figs. 5(a) and 5(c)] and the sinusoidal [Figs. 5(b) and 5(d)] gratings, respectively.

In the case of rectangular gratings, an extinction ratio as high as 25 dB for the Bragg band-rejection filter is achieved already with the smallest modulation amplitude, Δw = 50 nm. Further increases in Δw yield only marginal improvements, as the extinction ratios essentially saturate at values around 27 dB, without exhibiting a consistent monotonic trend. On the contrary, in the case of sinusoidal gratings the amplitude of the transmission dip steadily increases with Δw, reaching a maximum extinction ratio of 24.2 dB for Δw = 125 nm. The measured extinction ratios are significantly higher than those previously obtained with Bragg gratings in LN waveguides (~18 dB, over a bandwidth of ~280 nm [16]) and appear in line with recent achievements in high confinement waveguide structures in silicon-on-insulator (SOI), providing a clear indication of operation in the strong coupling regime [4].

Optics EXPRESS

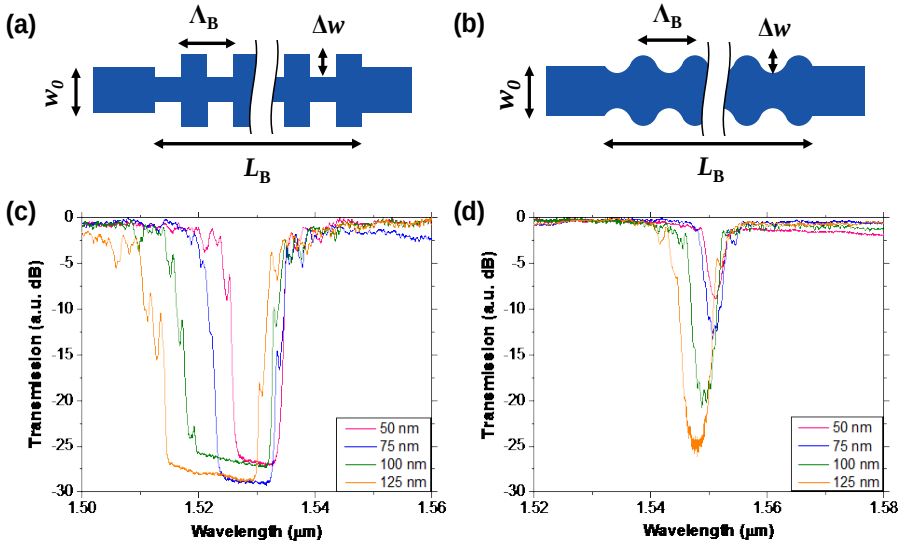

Fig. 5. Schematic top view illustration of Bragg gratings with (a) rectangular, and (b) sinusoidal-sidewall modulations. Normalized transmission curves obtained from measurements in the telecom range on 252.5 μm-long Bragg gratings with different waveguide width corrugations (Δw, color coding in the legend) for: (c) rectangular, and (d) sinusoidal grating profiles.

The saturation effects arising in the rectangular LNOI Bragg gratings [Fig. 5(a)] closely resemble the response recently observed with SOI Bragg gratings in the strong coupling regime, where maximum achievable extinction ratios appear to be limited by additional losses associated with scattering at the grating sidewalls, an effect which becomes more pronounced for increasing corrugation amplitudes Δw and which is enhanced by the abrupt discontinuities in the rectangular profiles [4, 29]. Moreover, additional contributions to the above saturation effects may arise from a non-perfect control of the polarization state at the device input (due to the use of non-polarization maintaining fibres) and in propagation (due to possible scattering at waveguide imperfections). The sinusoidal gratings provide also substantially narrower full-width-at-half-maximum (FWHM) bandwidths ($\Delta\lambda_{FWHM}$) than the rectangular ones, in good agreement with theoretical predictions [30]. For both grating typologies, $\Delta\lambda_{FWHM}$ increases with the Bragg corrugation Δw. The broadening is more pronounced in the rectangular structures, where $\Delta\lambda_{FWHM}$ increases from 10.8 nm to 23 nm as Δw is increased from 50 nm to 125 nm. In both grating structures, an increase of the grating corrugation, Δw, is also accompanied by a progressive blue-shift of the central wavelength of the Bragg filter (λ_0). This feature is also an indicator of operation in the strong coupling (perturbative) regime, as discussed further in the analysis section.

Finally, the impact of increasing grating lengths on the Bragg filter response was also experimentally investigated by fabricating and characterizing sinusoidal Bragg gratings which were twice as long. The overall outcomes of the measurements performed for the two different grating lengths (L_B = 252.5 μm and 505 μm) are summarized in Fig. 6. The grating performance in the two cases (square and circular markers) is quantified in terms of their 3 dB-bandwidths and extinction ratios, plotted together (in red and blue, respectively) as functions of Δw. Both grating lengths yield a monotonic increase of the bandwidth with Δw, in agreement with what discussed for Fig. 5(b). For Δw = 50 nm, the bandwidth does not change substantially as the grating length is doubled, which is consistent with the theoretical expectations for ideal Bragg structures in the strong coupling regime (Eq. (67) in [31]). However, for larger values of Δw, the longer gratings appear to exhibit overall slightly larger bandwidths, an effect which (similarly to the extinction ratio saturation in Fig. 5(a)) can be

Optics EXPRESS

attributed to the increasing scattering losses at the Bragg grating interfaces occurring for higher values of Δw, not accounted by the standard model of [31].

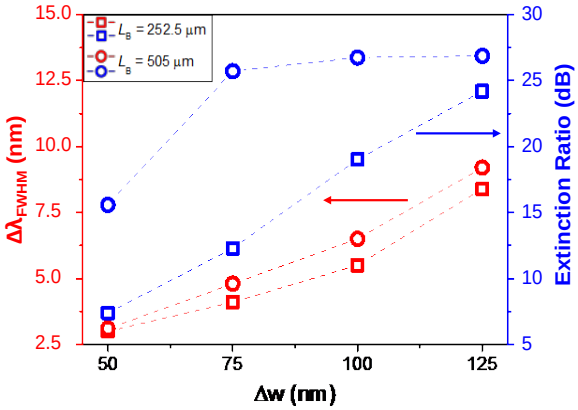

Fig. 6. 3dB bandwidth and extinction ratios experimentally obtained from Bragg reflectors with sinusoidal sidewall modulations, of length L_B = 252.5 µm (squares) and L_B = 505 µm (circles), as functions of the grating corrugation Δw.

The extinction ratios measured for the 505 µm-long Bragg gratings are approximately twice those recorded for gratings which are half this length, when Δw = 50 nm and 75 nm. As Δw is further increased, the measured extinction ratios tend to saturate to approximately 27 dB, similarly to what observed for the rectangular gratings and discussed with reference to Fig. 5(a). The optimal performance of the sinusoidal Bragg gratings in the diagram of Fig. 6 is achieved with a 505 µm-long Bragg grating structure for Δw = 75 nm, yielding an extinction ratio of 25.7 dB while still retaining good spectral selectivity, i.e. a 3dB-bandwidth of 4.77 nm.

4. Numerical analysis

To gain further insight into the performance of the Bragg gratings, the experimental results were compared with the predictions of different semi-analytical and numerical models routinely used for the analysis of integrated Bragg grating structures. This included a first, more intuitive treatment of the Bragg gratings based on coupled mode theory (CMT) [30, 31] followed by a numerical analysis by transfer matrix methods (TMM) in waveguide configuration [32].

For the sake of simplicity, the general trends in the expected performance of the Bragg gratings are first intuitively discussed with reference to single-mode lossless structures, where a simple relation links the response of the Bragg grating in reflection and transmission, and semi-analytical expressions describing the impact of different parameters on the grating response are readily available [30, 31]. A key parameter, quantifying the '*strength*' of a Bragg grating is its coupling coefficient, κ [3, 30, 31]. In the specific case of our sidewall gratings implemented with single-mode LNOI waveguides, the computed values of κL_B are in the range of 1.5–6.9, most of which correspond to gratings with κL_B>3, the so-called strong grating regime [2]. This assumption is fully consistent with the trend experimentally observed for the Bragg rejection bandwidth ($\Delta\lambda_{FWHM}$) as a function of the grating corrugation amplitude (Δw), given that in the strong coupling regime the former should theoretically grow with κ (Eq. (67) in [31]). The latter is essentially a measure of the overlap of the guided mode distribution with the index modulation (Eq. (56) in [31] or Eq. (41) in [32] in CMT or TMM models, respectively), and hence is expected to increase with the sidewall corrugation. Moreover, for the same value of Δw, the coupling coefficient κ of a sinusoidally-modulated Bragg grating is smaller than its rectangular counterpart [30], which justifies the narrower bandwidths seen in the experiments with the sinusoidal gratings, presented in Figs. 5(c) and

Optics EXPRESS

5(d). The value of κ also affects the maximum reflectivity of a Bragg grating, hence the extinction ratios of its response as a spectral rejection filter in transmission. The maximum reflectivity of a Bragg grating (at phase-matching) is $R_{max} = \left|\tanh \kappa L_B\right|^2$ [30–32]. Therefore, in good agreement with the data shown by Fig. 5(d), increments in κ, which can be caused by raising Δw, result in higher extinction ratios. Also, as confirmed by the data in Fig. 6, increasing Bragg lengths L_B, yield increasing extinction ratios, until the onset of saturation effects (due to additional scattering losses not accounted by standard Bragg grating models).

The observed experimental shift of the Bragg wavelength (λ_0) for increasing modulation amplitudes (Δw) cannot be accounted by standard coupled-mode theory (CMT), which relies on a perturbative approach. In fact, CMT would predict a constant value of λ_0 in our structures, namely: $\lambda_0 = 2N\Lambda_B$, uniquely determined by the grating period (Λ_B) and the effective index (N) of the unperturbed waveguide of width w_0. The blue-shift of λ_0 seen in the experiments for increasing Δw is instead correctly reproduced by the TMM approach, where λ_0 is given by $\lambda_0 = 4\Lambda_B / \left(\frac{1}{N^+} + \frac{1}{N^-}\right)$, N^+ and N^- being the effective indices in the wider ($w = w_0 + \Delta w$) and narrower ($w = w_0 - \Delta w$) waveguide sections of the Bragg structure, respectively [32]. Since the waveguide dispersion is typically stronger in the narrower waveguides, the dependence on Δw is dominated by N^-, leading to a progressive decrease of λ_0 when Δw increases.

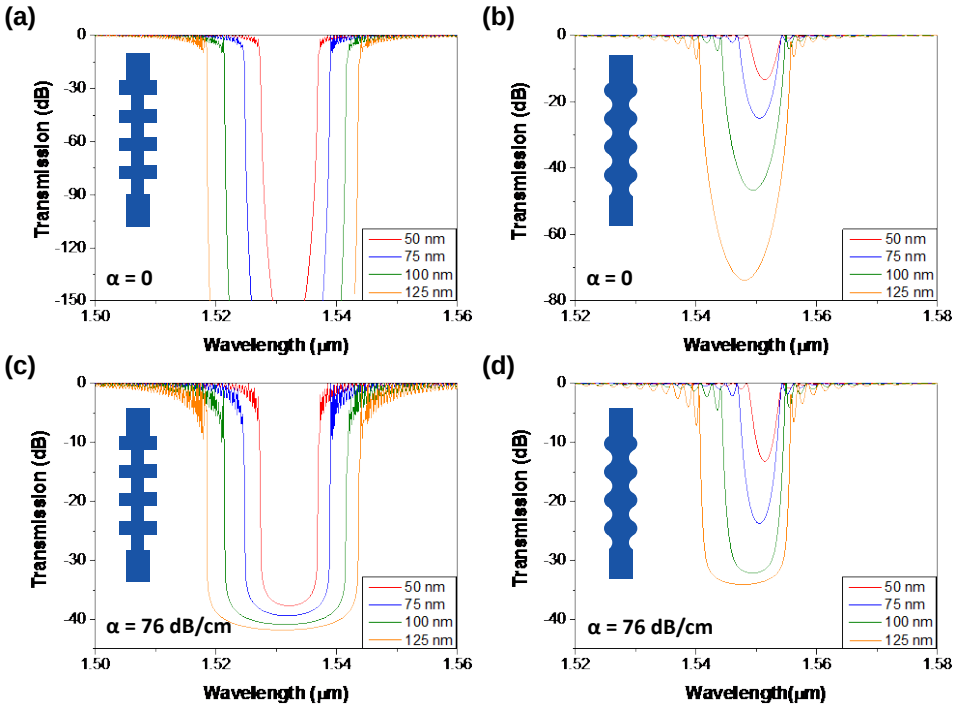

Fig. 7. Simulation results for Bragg gratings over a length of 252.5 μm for different waveguide width corrugations (Δw, color coding in the legend): (a-b) without propagation loss and (c-d) with propagation loss, for the rectangular (a,c) and the sinusoidal (b,d) grating structures of the experiments of Fig. 5.

Finally, in Figs. 7(a) and 7(b) we present the results of numerical simulations based on TMM, performed for the grating structures presented in the experiments of Fig. 5, assuming waveguides with no propagation loss. Overall, a good quantitative agreement is obtained for the 3dB bandwidths, spectral shapes of the transmission dip and location of the central

Optics EXPRESS

wavelengths. Nevertheless, a significant discrepancy is apparent in the values of the extinction ratios predicted by the simulations and seen in the experiments. This is essentially due to the fact that the propagation loss was ignored in this case. Simulations based on TMM models, suitably modified so to account for the propagation losses measured in uniform waveguides and also sinusoidal grating profiles appear more suitable to obtain more realistic values of the extinction ratios, as illustrated by the plots in Figs. 7(c) and 7(d). The remaining discrepancy of around ~10 dB between the theoretical and experimental values is justified by the limit in the experimental detection sensitivities and by the additional scattering losses expected for strong gratings in high confinement waveguides [29], not included in conventional models.

5. Conclusions

We presented a systematic experimental and theoretical study exploring high-contrast distributed Bragg gratings implemented in a thin-film LN platform. An optimized single-step electron-beam lithography and etching process was used to simultaneously fabricate high confinement sub-μm photonic wires and short-pitch Bragg gratings together with input/output tapers and grating couplers for efficient off-chip interfacing with standard telecom fibers. The experimental and theoretical analyses included also a characterization of the response of the nanowaveguides and of their wideband grating couplers, exhibiting a 3-dB bandwidth wider than 80 nm and fiber-to-waveguide coupling efficiency of ~–10 dB), employed to couple TE-polarized light into and out of the Bragg waveguide sections on chip. Bragg gratings realized through sinusoidal and rectangular sidewall modulations were designed, fabricated and characterized for their operation as rejection filters at telecom wavelengths in single-mode sub-μm LN waveguides. The experiments yielded extinction ratios in excess of 25 dB for ~250 μm-long rectangular gratings and slightly smaller values (24.2 dB) for sinusoidal gratings. The latter, however, featured narrower bandwidths (as small as 3 nm for the smallest Bragg corrugation) and limited saturation in the notch filter response. TMM-based simulations performed for the different fabricated structures showed a good agreement with the experimental results. The results could be easily transposed to TM-mode selective Bragg grating devices by using relief gratings, in analogy to work done in SOI [4].

In conclusion, the integrated Bragg grating devices demonstrated here on the thin-film LN platform pave the way towards the effective implementation of more advanced photonic designs which integrate the spectral and spatial tailoring functionalities of Bragg structures with the appealing nonlinear and electro-optic features of LN high confinement waveguides. Examples of perspective devices include phase-shifted Bragg grating structures and electro-optically tunable filters, to be potentially combined with e.g. 1D waveguide cavities for enhanced nonlinear effects and hence enable ultrasmall footprints in devices such as optical parametric oscillators and on-chip entangled photon sources.

Funding

Swedish Research Council (2-2010-526, 621-2014-5407, 621-2012-5364).

Acknowledgments

We gratefully acknowledge the kind assistance of Dr. Lech Wosinski facilitating the experiments and support from the Swedish Research Council (projects no. 621-2014-5407 and 621-2012-5364, and K.G.'s Rådsforskare Fellowship, no. 622-2010-526) and the ADOPT Linnaeus Centre in Stockholm. Portions of this work were presented at the CLEO-Europe conference in June 2017, in the oral contribution entitled: "*Waveguide gratings in thin-film lithium niobate on insulator*", Paper no. CK-2.6.